




Smoldering of Wood: Effects of Wind and Fuel Geometry

Luca Carmignani ^{*}, University of California Agriculture and Natural Resources, 7601 Irvine Blvd, Irvine, USA; University of California, Berkeley, University Avenue and, Oxford St, Berkeley, USA
Mohammadhadi Hajilou, University of Portland, Shiley School of Engineering, 5000 N. Willamette Blvd, Portland, USA
Jeanette Cobian-Iñiguez, University of California, Merced, 5200 Lake Rd, Merced, USA
Mark Finney, USDA Forest Service, Rocky Mountain Research Station, Missoula, MT 59808, USA
Scott L. Stephens, Michael J. Gollner and Carlos Fernandez-Pello, University of California, Berkeley, University Avenue and, Oxford St, Berkeley, USA

Received: 10 August 2023/**Accepted:** 2 January 2024

Abstract. Large and downed woody fuels remaining behind a wildfire's flame front tend to burn in a smoldering regime, producing large quantities of toxic gases and particulate emissions, which deteriorates air quality and compromises human health. Smoldering burning rates are affected by fuel type and size, the amount of oxygen reaching the surface, and heat losses to the surroundings. An external wind has the dual effects of bringing fresh oxidizer to the fuel surface and porous interior, while at the same time enhancing convective cooling. In this work, a series of experiments were conducted on single and adjacent poplar dowels to investigate the effect of fuel geometry and wind speed on smoldering of woody fuels, including its burning rate and combustion products. Dowels had variable thickness (19.1 and 25.4 mm), aspect ratios, and arrangement (number of dowels and spacing between them). Using measurement of mass loss, CO, and HC production as indicators of the smoldering intensity, the results indicate that the arrangement of smoldering objects significantly affects burning rates and emissions. Specifically, spacings of 1/8 and 1/4 of the dowel thickness enhanced the smoldering process. The smoldering intensity was also enhanced by increased external wind (ranging between 0.3 m/s and 1.5 m/s), but its effect was dependent upon the spacing between the dowels. The convective losses associated with the spacing were further investigated with a simplified computational model. The simulations show that the wind significantly increases convective losses from the smoldering surfaces, which in turn may offset the increase in smoldering intensity related to the higher oxygen flux at higher wind speeds.

Keywords: Smoldering, Wildfires, Heat transfer, Wood

^{*} Correspondence should be addressed to: Luca Carmignani, E-mail: carmignani@ucanr.edu, luca.carmignani@berkeley.edu



1. Introduction

Over the past decade, California and other Western regions of the United States have experienced increased tree mortality, leading to an accumulation of downed woody fuels on forest floors [1]. Unlike fine grasses and shrubs, which are typically consumed quickly by the flaming front of a wildfire, downed woody fuels can burn by smoldering for an extended period of time. The increased thickness and high density of large diameter woody fuels makes flaming ignition and sustained burning difficult, often leaving significant quantities of unburned fuels in the post-fire front. Despite the lower intensity of smoldering combustion, these accumulated fuels can still release more heat and emissions over time than living vegetation due to their large remaining fuel load, making final extinguishment more difficult [2]. These additional fuel loads can also affect the accuracy of predictive models of fire spread, as they typically only consider the heat released by the main, flaming fire front, not the post-frontal combustion region that can sometimes extend the burning region over a wide area rather than a traditional “fireline” [3].

Due to their nature, large, downed fuels tend to burn in the smoldering regime rather than in flaming mode, especially after a fire front has passed. In contrast to flaming, smoldering is a low-intensity type of combustion, and is controlled by the amount of oxygen reaching the burning surface as well as the amount of heat transferred to the surrounding environment [4–7]. In woody fuels, smoldering occurs when the char layer oxidizes, releasing heat and ash, and is often seen as the residual process of the flaming phase. However, smoldering can also occur independently as a self-sustained process due to its lower ignition temperature [8–11]. In internal crevices, a smoldering front can slowly spread for a prolonged period without being detected. An example is what happened to a giant sequoia in California’s Sequoia National Forest found to be burning several months after the Castle fire in 2020 [12]. Under certain conditions, the flammable gases produced during the pyrolysis process mixed with fresh air can ignite, resulting in the transition from a smoldering surface to a flaming fire [7, 13–15]. For non-homogeneous fuels such as wood, the intensity of smoldering and its potential transition to flaming depends on several factors such as wind, fuel size, and heat losses to the surroundings [6–9, 16, 17]. Several smoldering combustion reviews have been published [6–8, 10, 15].

Palmer and Perry [18] first studied the smoldering of fiber board strips under an external wind between 0.7 m/s and 2.6 m/s, concluding that the air flow was beneficial for the smoldering propagation rate and could lead to flaming, but its effect would also depend on the size of the fiber board samples. Ohlemiller and Schaub [19, 20] later investigated the smoldering of red oak and white pine boards arranged in U-shape channels. Self-sustained smoldering was observed for a narrow range of wind speeds (from 0.09 m/s to 0.22 m/s), and both wood types showed a similar increase in the smoldering spread rate with wind speed. These experiments showed that the process was not only controlled by the amount of oxidizer from the air supply reaching the fuel surface, but also by radiative and convective heat

transfer between the internal surfaces of the channels. Surface interaction is particularly important when considering the smoldering ignition of internal crevices [16, 21, 22]. The experiments from Richter et al. [22] showed that the chances of smoldering ignition from firebrand accumulating in crevices between flat wooden samples increase with wind speed (between 0.5 m/s and 1.4 m/s) but depend on the orientation between wind and crevice. The importance of surface interaction was also determined by Kwon and Liao [23], who examined woody samples (cubes of 19.1 mm) arranged in a 33 configuration with spacings up to 30 mm. In these experiments, smoldering was the residual process after the flaming phase. With increasing spacing, the surface temperature and mass consumption fractions of the cubes exhibited a non-monotonic trend, reaching maximum values at a spacing of 5 mm. Cobian-Iñiguez et al. [24] studied the effect of wind speed and fuel porosity on the smoldering rate of wooden cribs. For this geometry, wind speeds on the order of 1 m/s were beneficial for the smoldering process (measured in terms of mass loss and CO production rates), but fuel porosity did not seem to have a large impact on the results due to the large void fraction of the cribs. Porosity and air flow had higher impact on woody fuel beds such as pine bark [25], peat [26, 27], and incense [28]; these studies also showed the importance of sample size and geometry on the heat losses to the surrounding environment and thus the sustainability of the smoldering process. The forced air flow through the porous fuels was beneficial at low and intermediate velocities, in analogy with other non-woody fuels such as polyurethane foam [29, 30], but high velocities eventually led to blow-off extinction. However, the range of flow velocities varied greatly between studies due to the differences in fuel geometry and spreading configuration.

Despite the impact on fire behavior and emissions predictions, few studies have investigated the interlinked effects of wind speed and fuel geometry on smoldering of solid wood. In this work, we experimentally investigate the conditions under which smoldering can be self-sustained. Square poplar dowels with different thickness (19.1 and 25.4 mm), aspect ratio (length/thickness), and arrangement (single and multiple adjacent dowels, and two dowels with spacings between $1/8$ and $1/2$ of their thickness) are tested at wind speeds ranging between 0.3 m/s and 1.5 m/s. The effect of spacing between dowels is investigated by presenting experimental measurements of mass loss, CO, and HC production rates, which are compared for the two dowel thicknesses to estimate the intensity of the smoldering rate at the different wind speeds. Furthermore, to better interpret the experimental results, a computational model is used to evaluate the effects of the spacing and wind speed on the heat transfer between the sample surfaces.

2. Experimental Method

Experiments were performed in an enclosed wind tunnel shown in Figure 1. With reference to Figure 1, the wind direction is from right to left and generated by adjusting the upstream pressure of compressed dry air. Before entering the test section (highlighted by the red dashed box in Figure 1b), the compressed air is

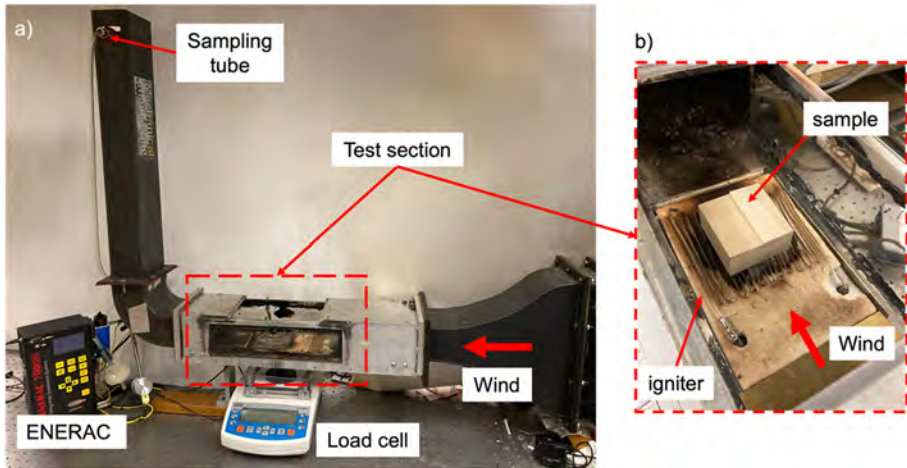


Figure 1. (a) Photograph of the experimental setup; (b) photograph of the test section showing a sample (consisting of two adjacent dowels) on top of the electrical igniter attached to the insulation plate, which is connected to the load cell.

injected into a plenum, passed through a series of glass beads and screens, then a contracting duct to ensure uniform airflow, with a maximum velocity of 1.5 m/s. The horizontal test section measures 13 cm (width) 10 cm (height) 35 cm (length), has an opening at the bottom for the sample holder, and one at the top to allow the samples to be changed (covered by a lid during the tests). After the test section the flow exists the tunnel through a vertical section (Figure 1a); the sampling probe of a gas analyzer (ENERAC 700) was mounted at the end of the vertical outlet to measure the post-combustion volumetric concentrations of CO, CO₂, and HC at 1 Hz. The CO and HC sensors could measure volumetric concentrations as low as 1 ppm, whereas the CO₂ sensor could detect volumetric concentrations above 10³ ppm.

A sample holder was mounted on the bottom surface of the test section and included an insulation plate mounted on a metal holder connected to a load cell, and an electrical igniter (17 AWG Nichrome wire wrapped into an S-shape, covering an area of approximately 7676 mm) stapled to the top of the insulation plate to ensure its surface was flat (see Figure 1b). The samples, consisting of square poplar dowels of two thicknesses (19.1 and 25.4 mm), and three aspect ratios (defined as length vs thickness, with the length of the dowels considered along the grain direction), were placed on top of the electrical igniter (direct contact) in a variety of arrangements (1–3 adjacent dowels, or two dowels with spacing), as illustrated schematically in Figure 2. To eliminate the influence of moisture content on the results, the dowels were dried at 105 °C for at least 24 h prior to the experiments (the measured moisture content was always less than 0.5%). Preliminary tests indicated that smoldering ignition could be achieved consistently by supplying a power of about 160 W for 300 s to the igniter at a constant wind speed

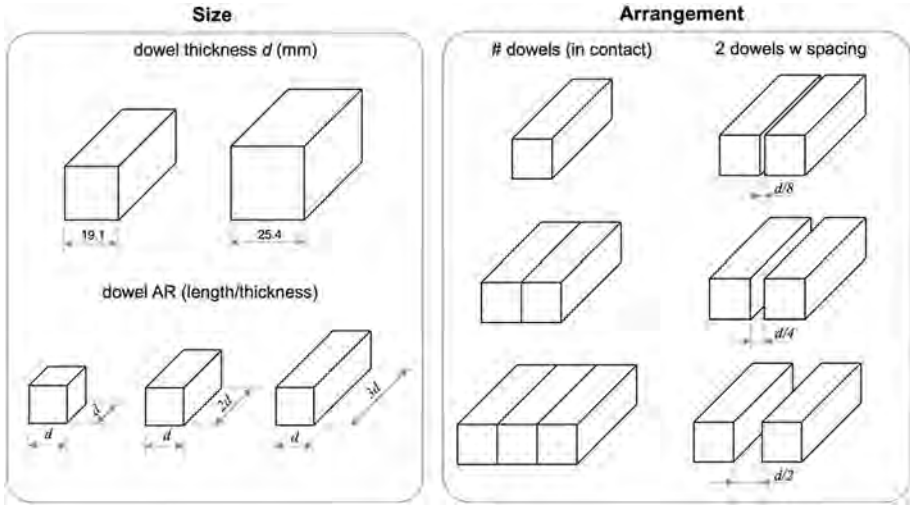


Figure 2. Experimental parameters.

of 0.2 m/s (to prevent smoke accumulation in the tunnel). Supplying more power to the igniter or using higher wind speeds often resulted in undesired flaming ignition. In some preliminary tests, the smoldering process stopped after the igniter was turned off; however, the same outcome was observed with longer ignition times or higher power. No significant differences were noticed in the power required to ignite samples of different size (thickness, length, arrangement). Therefore, it was concluded that the combination of power and time used in this study was appropriate to ignite the samples directly into a smoldering regime.

Experiments were conducted by placing the samples in the desired arrangement on top of the igniter at a wind speed of 0.2 m/s, and then turning on the igniter for 300 s. Afterwards, the igniter was turned off and the wind speed was adjusted to the desired value and maintained constant throughout the experiment. Wind speeds between 0.2 m/s and 1.5 m/s, with intervals of about 0.2 m/s were selected for the experiments. Once set to desired value, the wind speed fluctuation was less than 0.05 m/s. These wind speeds are representative of the wind that woody fuels would encounter close to the forest floor and would correspond to much higher values on top of the tree crowns. During a test, the load cell connected to the sample holder recorded the mass of the sample at 1 Hz with a resolution of 0.001 g. To account for the increase in mass caused by the force onto the load cell from the wind speed adjustment after ignition, the mass was recorded at the desired wind speed before ignition. The experiments were terminated when no significant change in mass was observed, or when the CO concentration in the exhaust flow dropped below 10 ppm. A minimum of two repetitions were conducted for all experimental conditions, with more repetitions carried out when the results were less consistent.

3. Results

Following the ignition phase (300 s), three possible outcomes were observed: (i) the samples stopped smoldering after the igniter was turned off (*no smoldering*); (ii) smoldering continued for less than ten minutes, but only in localized regions that eventually extinguished (*residual smoldering*); (iii) large areas of the samples kept smoldering for more than ten minutes (*self-sustained smoldering*).

3.1. Conditions for Self-Sustained Smoldering

The first objective of this study was to determine the conditions under which smoldering could be self-sustained. To compare the effect of the dowels' arrangement on the smoldering behavior, Figure 3 shows the results based on the surface area to volume ratio (SAV) of the samples without spacing, indicated separately for one (Figure 3a), two (Figure 3b), and three (Figure 3c) adjacent dowels with varying thickness and aspect ratio (parameters indicated in Figure 2). The diameter of each pie marker in Figure 3 is proportional to the number of repetitions of the experiment (with the smallest diameter corresponding to two repetitions), whereas the split represents their qualitative outcome (no smoldering, residual, and self-sustained smoldering). Single dowels (Figure 3a) did not sustain smoldering at any wind speed regardless of their size, with some residual smoldering observed at high wind speeds and lower values of SAV (thicker and longer dowels). Two adjacent dowels (Figure 3b) gave mixed results based on thickness and aspect ratio. However, even among repetitions of the same conditions, it was observed that the smoldering outcome would vary depending on the dowel position during the experiments. When they were almost completely in contact, there was no or residual smoldering, whereas when a small gap formed between them, there was residual or self-sustained smoldering. At a wind speed of 1.5 m/s, some of the samples with low SAV transitioned to flaming, as indicated by the red “” below the respective pie marker in Figure 3b. With three adjacent dowels (Figure 3c), self-sustained smoldering was obtained in every test. In several experiments, even at wind speeds of 0.3–0.7 m/s, the samples transitioned to flaming shortly after ignition. Additional tests at 1 m/s transitioned to flaming immediately after ignition, and since the focus of this study was the smoldering process, experiments at wind speeds higher than 0.7 m/s were not conducted. The dowel aspect ratio did not seem to play a role for longer dowels (AR 2 and 3), whereas dowels with an aspect ratio of 1 (cubic dowels) did not sustain smoldering even in multiple-dowel arrangements.

To further study the effects of geometry and wind speed on the dowels' self-sustained smoldering, additional experiments were carried out by introducing a spacing between two dowels, equal to 1/8, 1/4, and 1/2 of the thickness, d . For these experiments, only the longer dowels (AR of 3) were considered.

3.2. The Effect of Spacing

An example of the time evolution of a two-dowel sample with a thickness of 25.4 mm and a spacing of 3.2 mm ($d/8$) burning at a wind speed of 1.5 m/s, is

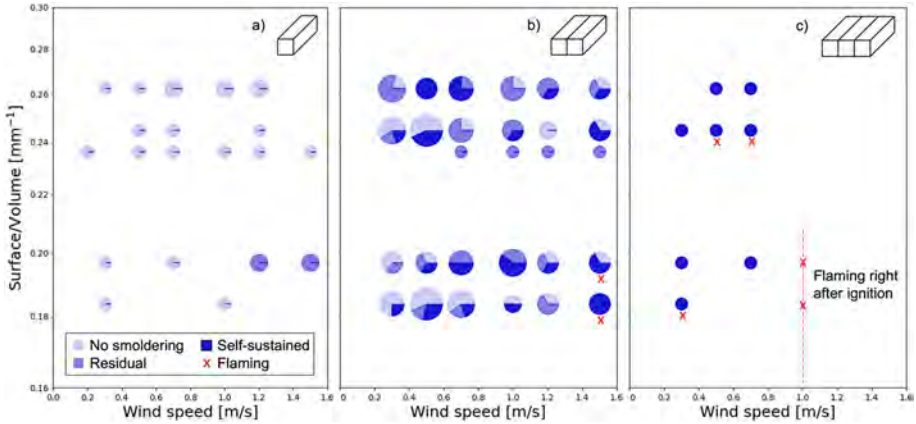


Figure 3. Smoldering behavior observed in the experiments based on surface area to volume ratio and wind speed for: (a) single dowels; (b) two, and (c) three adjacent dowels. The pie marker diameter corresponds to the number of repetitions of the same test (minimum of two repetitions), and the slices represent the fraction of the specific outcome (no smoldering, residual, self-sustained). The tests where transition to flaming was observed are indicated by a red “x” below the respective markers.

illustrated in Figure 4. The photographs of the sample in Figure 4a were taken at intervals of 200 s, whereas the graph in Figure 4b shows the variation of mass (left axis), and volumetric fractions of CO, CO₂, and HC (right axis, with CO and HC values multiplied by 10 for a better comparison with CO₂) measured over time. The reference time $t = 0$ corresponds to the time when the igniter was turned on (with a wind speed of 0.2 m/s). After the igniter was turned off ($t = 300$ s), the wind speed was increased to 1.5 m/s, which resulted in the increase in measured mass visible from the graph of Figure 4b, and the disappearance of the smoke between the images at 200 and 400 s (Figure 4a). Starting from the sample bottom surface, the smoldering front spread upward, with higher intensity closer to the spacing, as indicated by the reversed V-shape of the charred layer in the frontal section of the sample visible in Figure 4a ($t = 1000$ and 1200 s), and by post-experiment visual examination of samples from similar experiments manually terminated with nitrogen (Figure 4c). At about $t = 1400$ s, the sample transitioned to flaming (starting from the trailing edge of the sample), which lasted until $t \approx 1550$ s, as indicated by the sharp decrease in measured mass loss. The combustion products volumetric fractions quickly increased during the ignition phase. The CO sensor of the gas analyzer was often close to saturation during ignition, and it needed about 60 s to adjust after the igniter was turned off. After $t \approx 500$ s, the CO concentration steadily increases until 1400 s, while the HC volumetric fraction is almost constant, and no appreciable CO₂ was detected. During the flaming transition, the CO₂ fraction rapidly increases while the CO fraction drops. Similar trends of the emissions volumetric fractions were observed for the rest of the

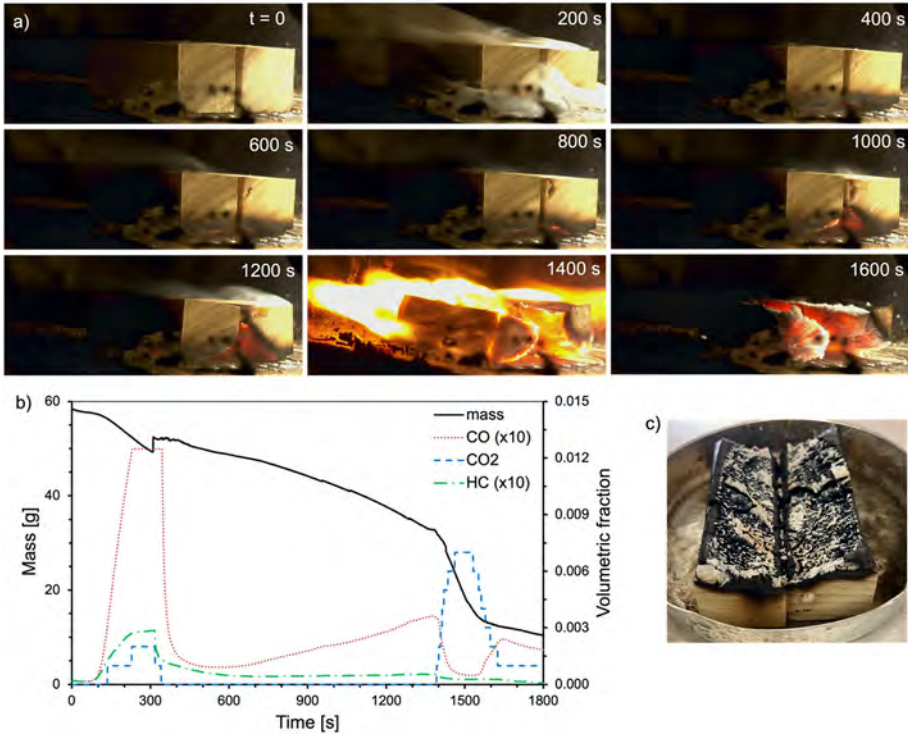


Figure 4. (a) Photographs of a sample exposed to a wind speed of 1.5 m/s with a time interval of 200 s; (b) variation in time of sample mass (with reference to the left axis), CO, CO₂, and HC volumetric fractions (with reference to the right axis). The values of CO and HC have been multiplied by 10 for a better visualization. (c) Picture of the bottom surface of a sample after an experiment; the entire surface smoldered, burning more material on the side facing the spacing between the dowels.

experiments, with appreciable increases of CO₂ detectable only during ignition and flaming transitions. This could be due to the sensitivity of the CO₂ sensor (smaller compared to the CO and HC sensors), indicating that during the dowel's smoldering phase the CO₂ values were below the minimum detectable volumetric fraction of 1000 ppm. For reference, the measured CO concentration was between 50 and 150 ppm in most experiments.

The experiments showed a linear decrease in mass over time, thus the mass loss rate was calculated as the slope of the curve after ignition. For consistency between the mass and gas measurements, and to avoid the influence of the ignition phase, the time range between 500s and 1000s was used to calculate the mass loss, CO, and HC production rates. The CO and HC volumetric fractions were converted to production rates by calculating the volumetric flow rate inside the tunnel test section at different wind speeds.

Each row of Figure 5 shows respectively the variation of mass loss rate, CO, and HC production rates with wind speed for the different spacing values (indicated in the legend), with the error bars indicating the standard deviation among test repetitions. The graphs on the left column are relative to the dowel thickness of $d = 19.1$ mm, whereas the graphs on the right column refer to $d = 25.4$ mm. The mass loss rate (Figure 5a) has similar values for the two thicknesses at low wind speeds, while at wind speeds larger than 0.7 m/s the thicker dowels (25.4 mm) show a much higher increase in mass loss rate. The CO (Figure 5b) and HC (Figure 5c) production rates, on the other hand, have similar increasing trends with wind speed, with larger values for the thicker dowels (25.4 mm). These general increasing trends with wind speed depend on the spacing between the dowels; intermediate spacing values ($d/8$ and $d/4$) in Figure 5 show the largest values for the mass loss rate, as well as the CO and HC production rates. The rates for “no spacing” and $d/2$ show instead lower values and trends, even though they are characterized by larger standard deviations. The variation in mass loss rate, CO, and HC production rates with wind speed observed in Figure 5 could be due to spacing-dependent heat losses, or the increased flux of oxidizer reaching the smoldering surface.

3.3. Computational Analysis

The presence of a spacing between two dowels introduces a thermal radiative exchange between the internal facing surfaces and influences the flow of oxidizer to the smoldering surface. However, the wind in the spacing also increases the convective cooling. The influence of the wind speed and the spacing between two dowels on the heating to the internal-facing surfaces was studied computationally with ANSYS Fluent to gain more insight into the effect of convective cooling versus thermal radiation. We considered the spacing between the two dowels as the domain of the problem, as shown in Figure 6, where an inlet velocity boundary condition was defined on the left side of the domain and set to the value used in the experiments, and the opposite and top surface of the computational domain included an atmospheric pressure boundary condition. During the experiments, especially in the time period between $t = 500$ and 1000 s, it was observed that the smoldering process would mostly occur in the lower section of the samples, as qualitatively shown in Figure 4c. To simulate this behavior computationally, the height of the domain was divided into a lower section ($1/3$ of the height) delivering a constant heat flux, and an upper section ($2/3$ of the height) at room temperature (Figure 6). The lower section of the internal surfaces was assumed to have a fixed and uniform heat flux of 6 kW/m^2 , based on the minimum value obtained by Liang et al. [31] to sustain the smoldering of a flat wood surface. The bottom surface of the domain was assumed adiabatic to simulate the insulation plate underneath the samples in the experimental configuration. The simulations were performed for both the dowel thicknesses of 19.1 mm and 25.4 mm, with their respective lengths of 57.2 mm and 76.2 mm (aspect ratio of 3). The spacing between the dowels included $1/8$, $1/4$, and $1/2$ of the dowel thicknesses.

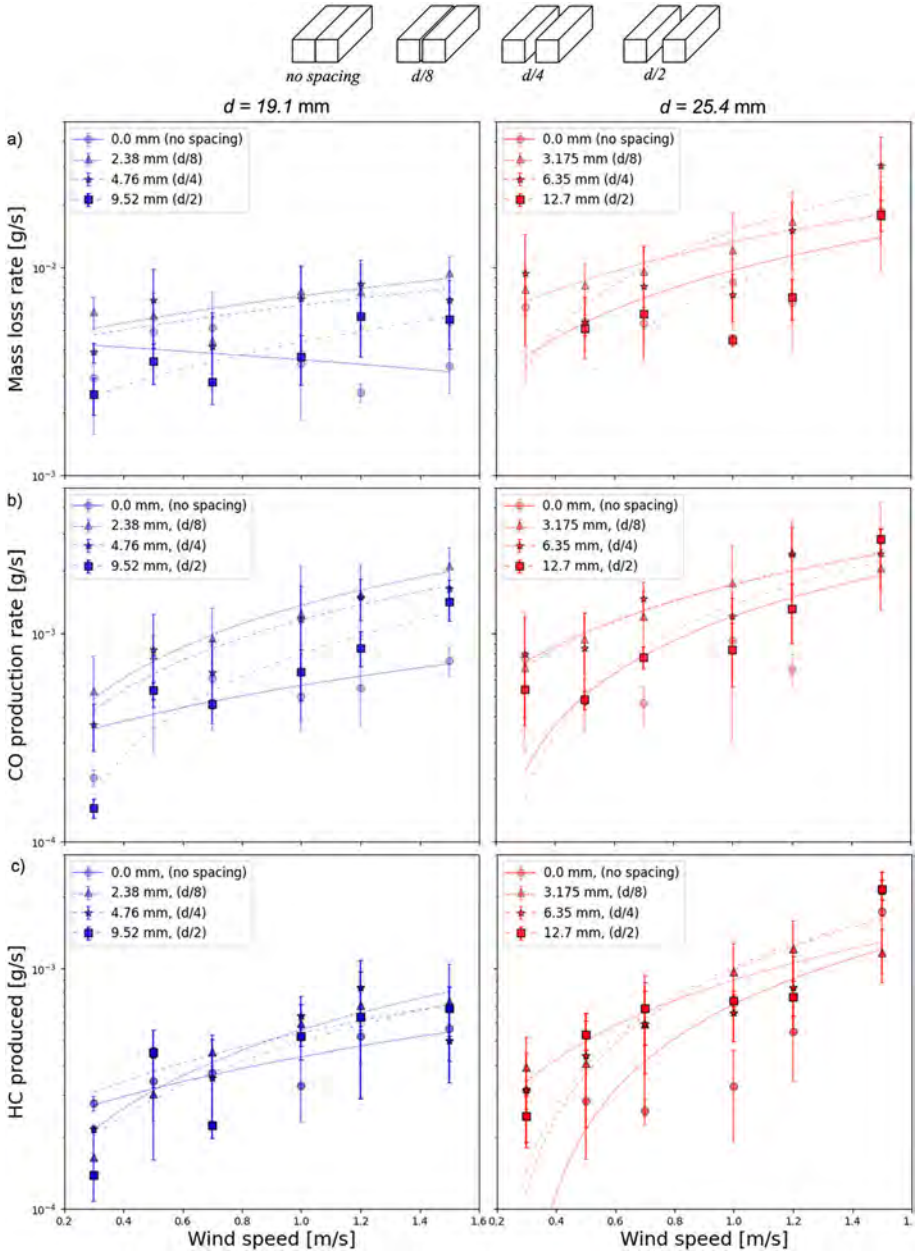


Figure 5. Effect of spacing and wind speed on: (a) average mass loss rate, (b) CO, and (c) HC production rates for dowels with thickness of (left column) 19.1 mm, and (right column) 25.4 mm.



Figure 6. Computational domain corresponding to the spacing between the dowels.

A mesh independence study was performed to choose the best mesh size for the simulations, and following this a time step study was performed using a Courant number of 0.8. These initial simulations resulted in choosing a structured mesh with a size of $6.7 \cdot 10^{-4}$ m. Additionally, a comparison between laminar and turbulent flow models in both transient and steady state conditions was performed, and it was observed that the obtained results are approximately the same for all these conditions; hence, laminar steady state conditions were used to simulate the problem. A Monte Carlo model was utilized to solve for radiation heat transfer between the surfaces. Furthermore, a coupled scheme was chosen to solve for the pressure–velocity coupling with second order upwind discretization method for both energy and momentum equations.

Figure 7 shows the comparison of contours of the radiation flux in the mid-plane of the considered geometry for two values of wind speed (0.5 and 1.0 m/s), and the three spacing values (2.4, 4.8, and 9.5 mm) for dowels with a thickness of 19.1 mm. The midplane was defined as the center of the computational domain in the numerical simulations. As can be qualitatively observed in these figures, most of the heating occurs in the downstream region of the domain, and higher wind speed and gap sizes result in smaller heat fluxes. This is the result of higher wind speeds enhancing the convective cooling of the internal-facing surfaces of the dowels, and the reduction in their radiative exchange due to the decreasing view factor for larger spacings.

The heat flux values in the middle plane (see Figure 7) were averaged over the entire plane surface for the comparison of all the conditions tested in the experiments. These computational results are reported in Figure 8 for the two dowel thicknesses and all the spacing values. The average heat fluxes show a sharp decrease with the wind speed (in particular, for the smallest spacings), which is consistent with what was qualitatively observed in Figure 7.

4. Discussion

The experimental results showed that smoldering combustion could not be sustained by single dowels (Figure 3a), or dowels with an aspect ratio of 1. The ignition protocol used in this work was first hypothesized to be responsible for this

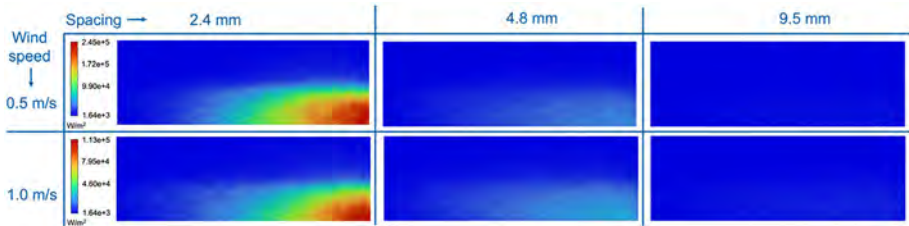


Figure 7. Radiation flux contours in the midplane of the domain (spacing between dowels) for dowels with a thickness of 19.1 mm exposed to a wind speed of (top) 0.5 m/s, and (bottom) 1 m/s.

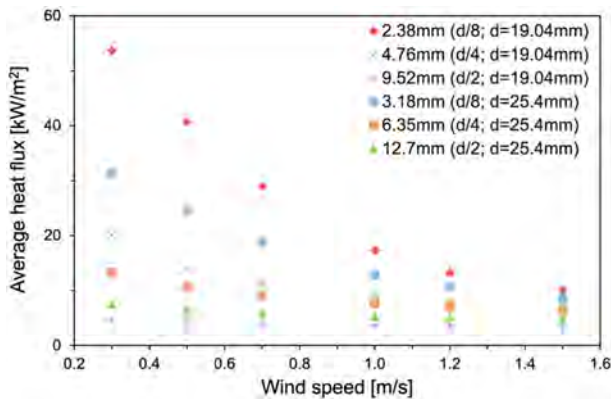


Figure 8. Heat flux averaged over the midplane of the domain for different values of spacing and thickness of the dowels, and wind speed.

outcome; however, additional experiments with the igniter running for up to 900 s or using a higher power showed that the samples just charred at the bottom and did not sustain smoldering. Hence, variations in ignition time and igniter power did not significantly affect these results. Furthermore, an approximate calculation of the igniter heating power across its area gives a heat flux of 25 kW/m^2 , similar to that reported in the literature for smoldering ignition (without flaming) [6–11].

The size of the dowels may have contributed to the no-smoldering results, particularly for thinner dowels. While thinner wooden disks were shown to smolder at a higher rate in the experiments of Wang et al. [32], those samples were exposed to an external heat flux, as opposed to our experiments where the external heat flux was applied only for 300 s and additional convective cooling was introduced by the external wind. Based on previous studies of the spread of a smoldering front over polyurethane foam [29, 33], Rein developed an expression to determine a critical length scale L_c (for a square-section prismatic sample) for the sample to achieve self-sustained smoldering [34]:

$$L_c = \frac{4\delta U_{\text{loss}}(T_s - T_0)}{Q_{sm} \dot{m}''_{O_2}}, \quad (1)$$

where δ is the thickness of the smoldering front, T_s and T_0 are respectively the surface and ambient temperatures, and U_{loss} is the overall heat loss coefficient. Q_{sm} is the heat released by the smoldering process per unit mass of oxygen, and \dot{m}''_{O_2} is the mass flux of oxidizer. The values from Boonmee and Quintiere [11] for the heat of combustion of the char layer, heat transfer coefficient for laminar convection over a flat plate, and surface temperature are, respectively, $Q_{sm} \sim 32.76 \text{ kJ/kg}$, $U_{\text{loss}} \sim 10 \text{ W}/(\text{m}^2\text{K})$, and $T_s \sim 500^\circ\text{C}$. Assuming a smoldering thickness of $\delta \sim 6 \text{ mm}$ (on the order of $d/3$ for a dowels thickness of 19.1 mm, based on experimental observations as in Figure 4c), and a mass flux corresponding to a wind speed of 0.3 m/s for atmospheric dry air, from Equation (1) we obtain a critical size $L_c \sim 50 \text{ mm}$ (for polyurethane foam, the critical size is approximately 160 mm [34]). Considering the size of the dowels tested in this study, this estimate may explain why even two adjacent dowels smoldered only in some cases; however, loose contact between adjacent dowels or a spacing in between facilitated the sustained smoldering of the samples.

With a spacing of 1/8 and 1/4 of the dowel thickness, smoldering was self-sustained at almost every wind speed. Adjacent dowels (no spacing), and the ones with a spacing of $d/2$ only sustained smoldering in some repetitions and mostly for wind speeds higher than 0.7 m/s. It is interesting to notice that similar trends with spacing were found for the smoldering of cubes (after the flaming phase) by Kwon and Liao [23], crevices and cracks on the wood surface [16, 17, 23], and wooden deck boards [21].

The data on mass loss rate in Figure 5 is scattered due to the nature of the smoldering process and the resolution of the load cell, but overall the values seem to increase with wind speed, especially for the dowels thickness $d = 25.4 \text{ mm}$. The values at high wind speeds are comparable to the ones measured by Liang et al. [31] for self-sustained smoldering of woody plates exposed to low irradiation. The increasing trend with the wind speed is clearer from the CO production rates, with the spacings of $d/8$ and $d/4$ showing the highest increase. According to these results, it is shown that (i) wind speed enhances smoldering between two dowels, in agreement with the crib results from Cobian-Iñiguez et al. [24], and (ii) a small spacing allows for better propagation of smoldering fronts. This spacing results in enhanced radiative exchange between the internal surfaces of the dowels, and an increase of fresh oxidizer reaching those surfaces, both of which facilitate the smoldering process. On the other hand, the spacing also results in higher convective cooling, especially at high wind speeds. Thus, the balance between those two effects determines if smoldering is enhanced or deterred.

The computational results indicate that convective cooling caused by the wind speed strongly reduces the average heat flux exchanged between the internal surfaces of the dowels (Figure 8). Spacings below 5 mm are the ones most affected by the increase in wind speed. The computational model, however, did not include the variation of oxidizer reaching the smoldering surface with wind speed, which

could enhance the surface temperature and burning rate [4–7], and thus the heat transfer between the internal surfaces. From the results of Figure 5, it is not possible to say if the increase in mass loss rate, CO and HC production at higher wind speeds is due to an increase in smoldering reaction rate, or to the combustion of a larger portion of the dowels. For a better comparison of the dowel thicknesses, the mass loss rates presented in Figure 5 were divided by the mass of the samples right after the ignition phase ($t = 300$ s), whereas the values of the CO production rates were normalized with the corresponding values of the mass loss rates, with the results shown in Figure 9. The normalized mass loss rate increases with wind speed in every case, but the slope seems to be larger for the thicker dowels (25.4 mm). The adjacent dowels (no spacing) with $d = 19.1$ mm show a decreasing trend; however, a closer look to the data points reveals a non-monotonic trend, likely due to variations in dowels contact during the experiments that affected the mass loss rate. The normalized CO production rate, on the other hand, shows a different behavior for the two thicknesses; the thinner dowels (19.1 mm) show an increase, whereas the thicker dowels (25.4 mm) show a clear decrease for every spacing except for the “no spacing” case. Overall, these results suggest that the smoldering rate decreases with wind speed for thinner dowels (since more CO is produced with reference to the mass loss rate), whereas the smoldering rate for thicker dowels slightly increases with the wind speed, with rates depending on the spacing between the dowels.

5. Conclusions

A parametric study of the dependence of smoldering of wooden dowels on their geometry and external wind speed was conducted experimentally. The selected parameters allowed us to analyze separately the effects of dowel size (thickness and length), and arrangements (single and multiple dowels) on the smoldering behavior of woody samples exposed to an external wind. The results show that for the present tests fuel geometry has a stronger impact than wind. Single dowels did not sustain smoldering, whereas two dowels with a spacing in between them show different behaviors based on fuel thickness, spacing, and wind speed. A computational model was developed to estimate the heat transfer between the internal surfaces of two dowels with different spacings, and the results indicate that the convective cooling of the internal-facing dowels surfaces strongly reduces the radiative heat transfer between the dowels (assuming a constant heat flux from the smoldering area), especially for small values of the spacing. Normalized values of mass loss and CO production rates used to estimate the intensity of the smoldering rate for the different samples show a different behavior with wind speed for the two thicknesses tested. The smoldering rate seems to decrease for the thinner dowels, in agreement with the computational results, whereas for thicker dowels the smoldering rate increases with wind speed. Considering both the computational and experimental results, it is concluded that for the fuel geometry studied in this work the increase in oxygen flux to the surface due to the higher wind speed is compensated by the increase in convective losses, resulting in a small

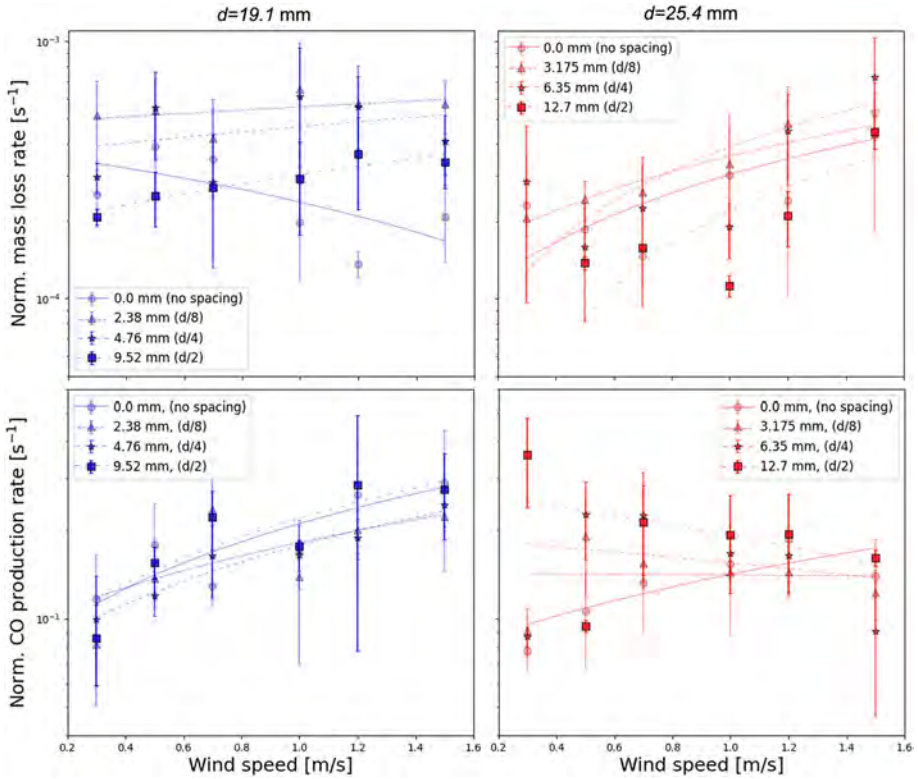


Figure 9. (top row) Normalized mass loss rate, and (bottom row) normalized CO production rate variations with wind speed for (left column) $d=19.1$ mm, and (right column) $d=25.4$ mm.

effect on the smoldering rate. Overall, the size and the geometry of the samples appear to have a stronger impact on the results than the wind speed, with small values of spacing ($d/8$ and $d/4$) and larger sample thicknesses facilitating the smoldering process. The experiments presented in this work could be easily expanded to study the range of geometry parameters that can affect the smoldering rate of woody fuels.

Acknowledgements

This work was supported by the California Energy Commission – Energy Program Investment Charge (EPIC) program [#EPC-18-026]. The authors thank Dr. Shaorun Lin for valuable comments on the manuscript, and Sitara Swaroop for helping with the experiments.

References

1. Stephens SL, Collins BM, Fettig CJ, Finney MA, Hoffman CM, Knapp EE, North MP, Safford H, Wayman RB (2018) Drought, tree mortality, and wildfire in forests adapted to frequent fire. *Bioscience* 68:77–88
2. North MP, Stephens SL, Collins BM, Agee JK, Applet G, Franklin JF, Fulé PZ (2015) Reform forest fire management. *Science* 349:1280–1281
3. Stephens SL, Bernal AA, Collins BM, Finney MA, Lautenberger C, Saah D (2022) Mass fire behavior created by extensive tree mortality and high tree density not predicted by operational fire behavior models in the southern Sierra Nevada. *Forest Ecol Manag* . [10.1016/j.foreco.2022.120258](https://doi.org/10.1016/j.foreco.2022.120258)
4. Parker AS, Hottel HC (1936) Combustion rate of carbon study of gas-film structure by microsampling. *Ind Eng Chem* 28:1334–1341
5. Evans DD, Emmons HW (1977) Combustion of wood charcoal. *Fire Saf J* 1:57–66
6. Ohlemiller TJ (2002) Smoldering combustion, Chapter 9 Section 2. *SFPE handbook of fire protection engineering*, 3rd edn. National Fire Protection Association, Quincy
7. Huang X, Gao J (2021) A review of near-limit opposed fire spread. *Fire Saf J* . [10.1016/j.firesaf.2020.103141](https://doi.org/10.1016/j.firesaf.2020.103141)
8. Babrauskas V (2002) Ignition of wood: a review of the state of the art. *J Fire Protect Eng* 12:163–189
9. Babrauskas V (2003) *Ignition handbook*. Fire Science Publishers, Issaquah
10. Rein G (2016) Smoldering combustion, Chapter 19. *sfpe handbook of fire protection engineering*, 3th edn. Springer, New York, pp 581–603
11. Boonmee N, Quintiere JG (2005) Glowing ignition of wood: the onset of surface combustion. *Proc Combust Inst* 30:2303–2310
12. The Guardian, Giant Sequoia found still smoldering after 2020 California wildfire (2021) <https://www.theguardian.com/us-news/2021/may/06/giant-sequoia-found-still-smoldering-after-2020-california-wildfire>. Accessed 29 Jan 2023
13. Tse SD, Fernandez-Pello AC, Miyasaka K (1996) Controlling mechanisms in the transition from smoldering to flaming of flexible polyurethane foam. *Symp Combust* 26:1505–1513
14. Santoso MA, Christensen EG, Yang J, Rein G (2019) Review of the transition from smoldering to flaming combustion in wildfires. *Front Mech Eng* 5:49. [10.3389/fmech.2019.00049](https://doi.org/10.3389/fmech.2019.00049)
15. Torero JL, Gerhard JI, Martins MF, Zaroni MAB, Rashwan TL, Brown JK (2020) Processes defining smoldering combustion: integrated review and synthesis. *Prog Energy Combust Sci* . [10.1016/j.pecs.2020.100869](https://doi.org/10.1016/j.pecs.2020.100869)
16. Zhang Z, Ding P, Wang S, Huang X (2023) Smoldering-to-flaming transition on wood induced by glowing char cracks and cross wind. *Fuel* . [10.1016/j.fuel.2023.129091](https://doi.org/10.1016/j.fuel.2023.129091)
17. Santoso MA, Christensen EG, Rein G (2023) The effects of pulsating wind on the transition from smoldering to flaming combustion. *Fire Saf J* . [10.1016/j.firesaf.2023.103993](https://doi.org/10.1016/j.firesaf.2023.103993)
18. Palmer KN, Perry MD (1953) Smoldering in dusts and fibrous materials Part VII: Fibre insulating boards under airflow conditions, F.R. Note 73. https://publications.iafs.org/publications/frn/73/-1/view/frn_73.pdf
19. Ohlemiller T, Shaub W (1988) Products of wood smolder and their relation to wood-burning stoves, National Bureau of Standards, NBSIR 88–3767
20. Ohlemiller TJ (1991) Smoldering combustion propagation on solid wood. *Fire Saf Sci* 3:565–574

21. Hedayati F, Quarles SL, Standohar-Alfano C (2022) Evaluating deck fire performance—Limitations of the test methods currently used in California’s building codes. *Fire* . [10.3390/fire5040107](https://doi.org/10.3390/fire5040107)
22. Richter F, Bathras B, Barbeta Duarte J, Gollner MJ (2022) The propensity of wooden crevices to smoldering ignition by firebrands. *Fire Technol* 58:2167–2188. [10.1007/s10694-022-01247-w](https://doi.org/10.1007/s10694-022-01247-w)
23. Kwon B, Liao YTT (2022) Effects of spacing on flaming and smoldering firebrands in Wildland-Urban interface fires. *J Fire Sci* 40(3):55–174. [10.1177/07349041221081998](https://doi.org/10.1177/07349041221081998)
24. Cobian-Iñiguez J, Richter F, Carmignani L, Liveretou C, Xiong H, Stephens S, Finney M, Gollner M, Fernandez-Pello C (2022) Wind effects on smoldering behavior of simulated wildland fuels. *Combust Sci Technol* . [10.1080/00102202.2021.2019239](https://doi.org/10.1080/00102202.2021.2019239)
25. Ronda A, Della Zassa M, Biasin A, Martin-Lara MA, Canu P (2017) Experimental investigation on the smoldering of pine bark. *Fuel* 193:81–94
26. Christensen EG, Hu Y, Purnomo DMJ, Rein G (2021) Influence of wind and slope on multidimensional smoldering peat fires. *Proc Combust Inst* 38:5033–5041
27. Lin S, Huang X (2021) Quenching of smoldering: effect of wall cooling on extinction. *Proc Combust Inst* 38:5015–5022
28. Lin S, Chow T, Huang X (2021) Smoldering propagation and blow-off on consolidated fuel under external airflow. *Combust Fl* . [10.1016/j.combustflame.2021.111685](https://doi.org/10.1016/j.combustflame.2021.111685)
29. Torero JL, Fernandez-Pello AC, Kitano M (1993) Opposed forced flow smoldering of polyurethane foam. *Combust Sci Technol* 91:95–117
30. Torero JL, Fernandez-Pello AC (1996) Forward smolder of polyurethane foam in a forced air flow. *Combust Fl* 106:89–109
31. Liang Z, Lin S, Huang X (2022) Smoldering ignition and emission dynamics of wood under low irradiation. *Fire Mater* . [10.1002/fam.3107](https://doi.org/10.1002/fam.3107)
32. Wang S, Ding P, Lin S, Gong J, Huang X (2021) Smoldering and flaming of disc wood particles under external radiation: autoignition and size effect. *Front Mech Eng* . [10.3389/fmech.2021.686638](https://doi.org/10.3389/fmech.2021.686638)
33. Bar-Ilan A, Rein G, Fernandez-Pello AC, Torero JL, Urban DL (2004) Forced forward smoldering experiments in microgravity. *Exp Thermal and Fluid Sci* 28:743–751
34. Rein G (2009) Smoldering combustion phenomena in science and technology. *Int Rev Chem Eng* 1:3–18

Publisher’s Note Springer Nature remains neutral with regard to jurisdictional claims in published maps and institutional affiliations.

Springer Nature or its licensor (e.g. a society or other partner) holds exclusive rights to this article under a publishing agreement with the author(s) or other rightsholder(s); author self-archiving of the accepted manuscript version of this article is solely governed by the terms of such publishing agreement and applicable law.